ACS OMEGA

http://pubs.acs.org/journal/acsodf

Article

Growth, Characterization, and Application of Vertically Aligned Carbon Nanotubes Using the RF-Magnetron Sputtering Method

Mikayel Aleksanyan, Artak Sayunts,* Gevorg Shahkhatuni, Zarine Simonyan, Hayk Kasparyan, and Dušan Kopecký

Cite This: *ACS Omega* 2023, 8, 20949−20958

Read Online

ACCESS | Metrics & More | Article Recommendations | Supporting Information

ABSTRACT: The aim of this work is to synthesize and characterize a nanostructured material with improved parameters suitable as a chemiresistive gas sensor sensitive to propylene glycol vapor (PGV). Thus, we demonstrate a simple and cost-effective technology to grow vertically aligned carbon nanotubes (CNTs) and fabricate a PGV sensor based on Fe_2O_3:ZnO/CNT material using the radio frequency magnetron sputtering method. The presence of vertically aligned carbon nanotubes on the Si(100) substrate was confirmed by scanning electron microscopy and Fourier transform infrared (FTIR), Raman, and energy-dispersive X-ray spectroscopies. The uniform distribution of elements in both CNTs and Fe_2O_3:ZnO materials was revealed by e-mapped images. The hexagonal shape of the ZnO material in the Fe_2O_3:ZnO structure and the interplanar spacing in the crystals were clearly visible by transmission electron microscopy images. The gas-sensing behavior of the Fe_2O_3:ZnO/CNT sensor toward PGV was investigated in the temperature range of 25−300 °C with and without ultraviolet (UV) irradiation. The sensor showed clear and repeatable response/recovery characteristics in the PGV range of 1.5−140 ppm, sufficient linearity of response/concentration dependence, and high selectivity both at 200 and 250 °C without UV radiation. This is a basis for concluding that the synthesized Fe_2O_3:ZnO/CNT structure is the best candidate for use in PGV sensors, which will allow its further successful application in real-life sensor systems.

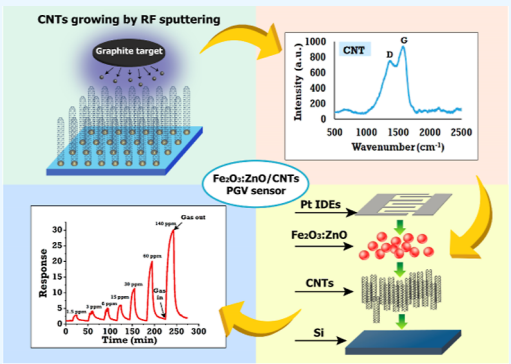

INTRODUCTION

As advanced materials with excellent physical, chemical, and mechanical properties, one-dimensional nanostructures have received incredible attention and applications in recent decades.[1,2] Among these structures, carbon-based nanostructures such as carbon nanocapsules, nanohorns, nanofibers, nanospheres, and carbon nanotubes (CNTs) are preferred due to their unique crystal structure and flexibility.[3,4] Compared to the structures listed above, CNTs are distinguished by their typical characteristics, which, since their discovery in 1991, have not lost their unique role in nanotechnologies.[5] High flexibility, elasticity, high surface area, excellent mechanical, tunable electrical, and ballistic transport properties make them the most promising nanostructures applicable in micro- and optoelectronics, high-speed memory devices, storage battery electrodes, sensor devices, and other related fields.[6−10]

CNTs are typically made up of hexagonal atomic layers of graphene rolled into a hollow cylindrical shape, while multiple tubes with slightly different diameters inserted into each other form multiwalled CNTs (MWCNTs).[11−16] The size and chirality of CNTs are largely determined by the type of the growing technology and its peculiarities, which in turn plays a decisive role in the acquisition of various types of nanotubes, such as metallic, semimetallic, or semiconducting properties.[17,18] The grown nanostructured material does not always contain the intended target structure in its entirety. In particular, nanorods, nanowires, and certain amorphous structures sometimes appear together with the grown CNTs. These are of course undesirable species, but if they are more closely related to CNTs, such as branched, coiled, bamboo-shaped, and toroidal CNTs, then they may have useful properties in specific applications, such as gas sensors, biosensors, etc.[19−24]

To choose the right technology for growing nanotubes, it is necessary to take into account the simplicity and cheapness of the given method and the quality of the nanotubes obtained by it. In the last decade, the growth of CNTs has been carried out mainly using the following technological methods: laser ablation, electric arc discharge (EAD), and chemical vapor deposition (CVD).[25−28] These methods have been well studied and greatly improved over the years to present a

Received: March 14, 2023
Accepted: May 22, 2023
Published: May 31, 2023

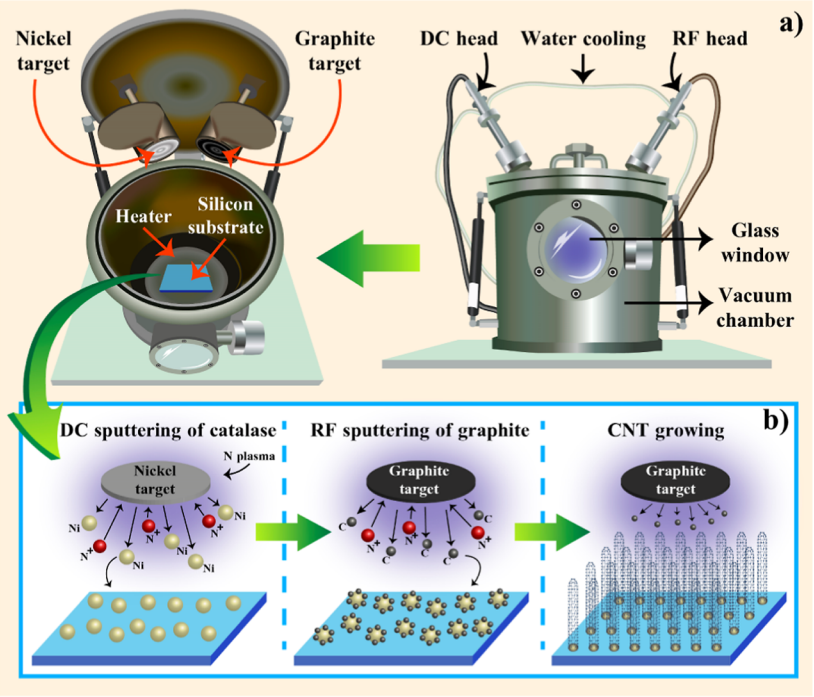

Figure 1. (a) Schematic illustration of the VTC-600-2HD DC/RF Dual-Head High-Vacuum Magnetron Plasma System and (b) representation of the CNT growing process.

high degree of crystallinity and purity. Despite all this, the growth of nanostructures by the above-mentioned techniques is accompanied by a low tunability and reproducibility of the key parameters of the growing nanotubes.[29−31] The high-frequency magnetron sputtering method represents a favorable alternative to obtaining CNTs as a simple and controllable growing technology. The noble gases used here, such as argon and nitrogen, as well as the graphite target for magnetron sputtering, have a fairly low price, which firmly lead to a low-cost technology. Furthermore, by using a two-head magnetron system [DC (direct current) and radio frequency (RF)], it is possible to perform both the catalytic element cluster deposition and nanotube growth processes in the same vacuum environment without additional oxidation risks.[23,32,33]

Propylene glycol (PG) is a colorless, water-soluble, and hygroscopic liquid with a distinctive glycol smell, low poisoning, low vapor pressure, and medium viscosity. PG serves as a nontoxic antifreeze in brake fluids and dairies and a substitute for ethylene glycol and glycerin. It is also used in food products as a humectant or as a solvent for artificial colorings and flavorings. PG is an important substance in the production of cosmetics and in various pharmaceutical formulations, including oral, injectable, or topical preparations. Besides, PG is extensively used in e-cigarettes, and the precise detection of its vapors can provide useful information on the composition and concentration of cigarette smoke.[34] This substance is also present in the vapors emitted from different types of food and drinks;[35−37] therefore, in electric noses, that determine the quality and freshness of food, the necessity of high-performance PG vapor (PGV) sensors is quite important. In e-nose systems, where dozens of sensors sensitive to different gases are integrated into a single detecting system, it is more important to apply sensors with high selectivity and a low detection limit. Therefore, selective and rapid detection of PGV and an accurate estimation of its low concentrations are now major challenges in various industries.[36−38]

The pristine metal oxides traditionally used in chemo-resistive gas sensors have been replaced by advanced nanocomposites, which are far superior in terms of their gas-sensing properties. Effective cooperation of carbon-based one-dimensional structures with the metal oxide compounds leads to their productive use in gas sensors, endowing them with a high speed, stability, and flexibility.[39−43]

In this work, we report the growth and characterization of vertically aligned CNTs synthesized by the RF magnetron sputtering method. We also fabricated a gas sensor based on Fe_2O_3:ZnO/CNTs material and studied its gas-sensing properties toward PGV at temperatures ranging from 25 to 350 °C with and without UV irradiation. The Fe_2O_3:ZnO/CNTs sensor showed a high performance toward PGV, confirming its applicability in sensor systems.

The nonexpensive and controllable method of the growing CNTs and the simple preparation technology of the Fe_2O_3:ZnO/CNTs sensor are attributed to a novelty managed to simultaneously have a high sensitivity to PGV, low detection limit, high response/recovery times, and low operating temperature, while there are now very few works in literature dedicated to the fabrication and investigation of PGV sensors.

EXPERIMENTAL SECTION

Growth of the CNTs by RF Sputtering. As one of the best physical vapor deposition techniques, the entire technological process of CNT growth was carried out by the factory-produced VTC-600-2HD DC/RF Dual-Head High-Vacuum Magnetron Plasma System (Figure S1).

The system allows us to control almost all parameters of growing nanotubes with high accuracy during sputtering. The system has DC and RF power supply blocks for the sputtering

https://doi.org/10.1021/acsomega.3c01705
ACS Omega 2023, 8, 20949−20958

Table 1. Sputtering Regimes for the CNT Growing Process

process	sputtering duration	generator power	working pressure (Pa)	sputtering gas	substrate temperature (°C)	cathode current	base pressure (Pa)
nickel sputtering (DC)	20 s		9.7×10^{-2}	nitrogen	400	300 mA	9.5×10^{-4}
graphite sputtering (RF)	3 h	100 W	5.1×10^{-2}	nitrogen	400		9.5×10^{-4}

of metal and semiconductor (or dielectric) targets, respectively.

CNTs were grown as follows. First, Ni catalytic nanoparticles were deposited on the substrate surface by DC power using a high-purity Ni target. After that, the high-purity graphite target was placed in the vacuum chamber on the RF head, which was bombarded with positive nitrogen ions. The heavy nitrogen ions were accelerated by magnetic and electric fields hitting the target. As a result, carbon atoms or nanoparticles were removed from the target and deposited on the substrate. The power of the magnetron sputtering generator was reduced to a point where it can still be sputtered as small particles as possible, or direct atoms were torn from the target, which were transported in a vacuum environment around deposited catalytic islands on the substrate growing vertically as nanotubes. The availability of two heads for DC and RF sputtering in the chamber allowed us to sputter metal nanoparticles and graphite in the same vacuum process, without transferring it through an air environment. The oxidation tendency of catalyst particles in the air environment sometimes leads to a stop or a decrease in the growth rate of nanotubes.[32] The schematic representation of the CNT growing process is shown in Figure 1.

The CNTs were grown by the RF sputtering method using previously purchased sputtering targets. The nickel and graphite targets (50 mm in diameter, N4 purity) were acquired by Changsha Xinkang Advanced Materials Co, Ltd (China) for the deposition of clusters of the catalytic element and the growth of CNTs, respectively. A Si(100) (Prime-Grade 2″ Silicon Wafers, N-Type, ρ = 10, Alpha Nanotech Inc., Canada) wafer was used as a substrate with a size of 10 × 12 × 1 mm. CNTs were grown simultaneously on the Si substrate with both smoothed and ragged sides during the same deposition process for further comparison (to highlight the effect of surface roughness on the CNT growth process). The silicon substrates were precleaned by boiling them in distilled water and in toluene for 2 and 3 h, respectively. Furthermore, they were kept in a vacuum environment for 30 min at 400 °C to remove surface oxygen species and other preabsorbed impurities from air. The base pressure in the chamber exceeded 9.5×10^{-4} Pa after 3 h of working of the turbomolecular pump. First, Ni catalytic particles were deposited onto the substrates using the DC head with a sputtering time of 20 s. Unlike other works,[23,33] in which catalyst particles were obtained by depositing a continuous metal layer on a substrate and then chemically etching them into islands, we obtained them during a short sputtering time. It is assumed that the extremely short sputtering time of Ni deposition did not allow for the formation of a continuous film but saturated the substrate surface with islands of metal particles that served as catalytic centers. It is known that among well-known catalysts (Fe, Co, Ni, Cu, etc.), nickel shows higher activity at lower temperatures (400−600 °C),[44−46] while we have grown CNTs at 400 °C. This definitely justifies the use of nickel particles as catalysts during the growth of CNTs, especially by the RF sputtering method.[33]

After that, the graphite particles were sputtered from the target through the RF head using nitrogen gas, which ensured the growth of nanotubes. It was confirmed[33] that the use of other gases, for example, argon, in the CNT growth process was not as efficient and led to a worsening in the crystalline perfection of the grown nanotubes. The whole sputtering regimes for the CNT growing process are summarized in Table 1.

Gas Sensor Fabrication. To prepare a sensor structure, Fe_2O_3:ZnO nanoparticles were deposited on the surface of the grown CNTs as a composite material with high sensitivity to PGV. The Fe_2O_3:ZnO nanoparticles were sputtered by the RF magnetron plasma system using the presynthesized Fe_2O_3:ZnO target.[47] Pt interdigitated electrode structures (IDEs) were deposited on the Fe_2O_3:ZnO/CNTs surface using a DC sputtering head to effectively record resistance changes in the sensitive film (Figure 2).

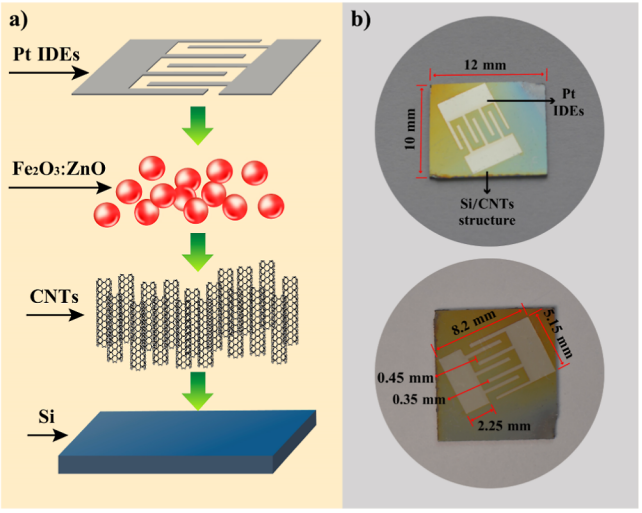

Figure 2. (a) Schematic representation and (b) actual photographs of the Fe_2O_3:ZnO/CNT sensor.

We used the following deposition regimes to obtain Fe_2O_3:ZnO nanograins. The base pressure in the vacuum chamber was 4.5×10^{-3} Pa, while during the deposition process, the chamber pressure was reduced to 5×10^{-1} Pa using an Ar gas flow of 30 SCCM. The substrate temperature was kept at 200 °C with a 12 cm distance between the substrate and the target. During the entire sputtering process (2 min), the cathode current was fixed at 250 mA, ensuring an uninterrupted deposition process. Finally, the sensor structure was kept at 300 °C for 4 h to obtain stabilized sensor parameters.

Gas-Sensing Setup. The gas-sensing behaviors of the Fe_2O_3:ZnO/CNTs sensor were investigated using a factory-designed GST PRO gas sensor testing system. The system has a cylindrical stainless-steel test chamber, in which a ceramic heater is attached keeping the sensor temperature from room temperature (RT) to 500 °C (Figure S2a). The testing system

https://doi.org/10.1021/acsomega.3c01705
ACS Omega 2023, 8, 20949−20958

is equipped with two gas insert channels with two mass flow controllers (MFCs) to mix and control gas flows (Figure S2b). The temperature and humidity sensors in the test chamber continuously monitor the actual temperature and humidity during the test process. All sensing parameters were registered by the PLC & HMI interface with a two-channel multimeter to read and log the output of gas sensors (R, IV) and PC-based software. A UV light-emitting diode (LED) (λ = 365 nm) is located 1 cm from the sensor surface with an illumination of 3 mW/cm^2. A liquid-phase vaporization system is also installed next to the chamber, which allows liquid PG to be vaporized and introduced into the chamber. The concentrations of PGV within the chamber were estimated using the proposed calculation method.[48] The definition of a gas response is given as follows: $S = R_{air}/R_{gas}$, where R_{air} and R_{gas} are the sensor electrical resistances in air and in the presence of PGV, respectively.

RESULTS AND DISCUSSION

Characterization. To confirm the influence of the surface roughness of the silicon substrate on the nanotube growing process, we used both smoothed and ragged sides of Si substrates in the same vacuum process [both sides of the Si substrate had (100) crystal orientation]. Scanning electron microscopy (SEM) images of the ragged surface of the substrate show that in this case, no nanotubes had grown on the substrate, but only an amorphous layer of graphite was deposited (Figure 3).

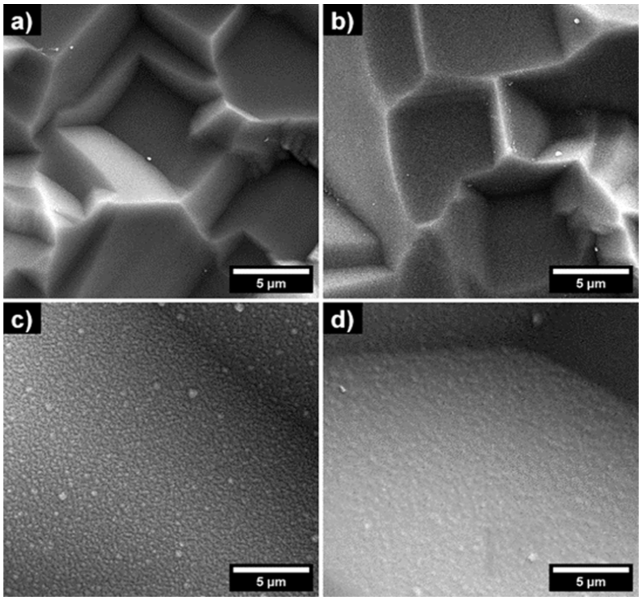

Figure 3. SEM images of the ragged side of the undeposited (a,c) and graphite-deposited (b,d) Si substrate.

The morphologies of the grown nanotubes on the Si(100) substrate and the undeposited surface were also investigated and compared using the SEM technique (Figure 4). Here, the presence of vertically aligned nanotubes is evident, which are believed to have a bamboo-like appearance.[32] The grown CNTs are quite homogeneous, which is attributed to the homogeneous distribution of the nickel catalyst particles on the Si(100) substrate. The diameters of the nanotubes do not differ significantly from each other and are in the range of 15−25 nm.

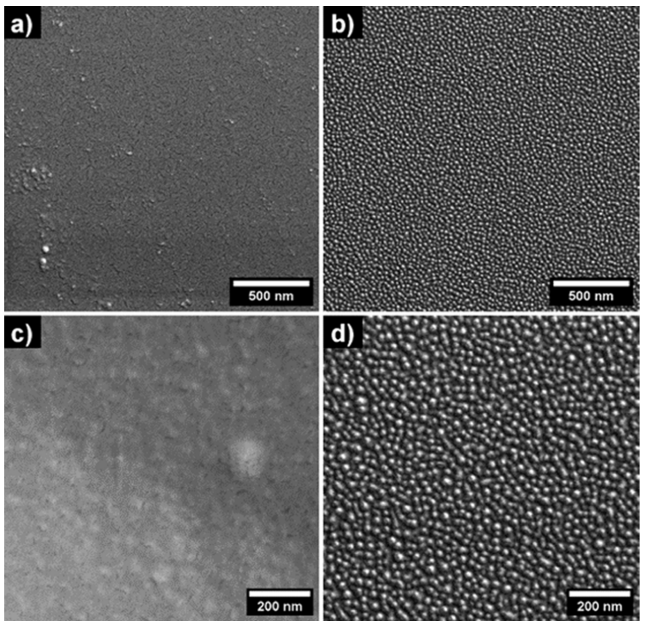

Figure 4. SEM images of the smoothed side of the undeposited (a,c) and CNT-grown Si(100) surface (b,d).

The CNTs/Si(100) structure was characterized by Raman spectroscopy using a DXR microscope (Figure S3). The presence of D (1367 cm^{-1}) and G (1580 cm^{-1}) bands was a typical characteristic of the formation of CNTs which were attributed to the disorder-induced active mode (D) and the graphite mode (G), respectively.[49] The appearance of the 500 cm^{-1} peak was a typical characteristic of a silicon substrate.[50] The well-pronounced intensity peaks of 1608 and 1192 cm^{-1} in the Fourier transform infrared (FTIR) spectrum of the CNTs/Si sample coincided with the G and D bands,[51] respectively, unequivocally confirming the formation of CNTs (Figure S4). The pronounced peaks below 900 cm^{-1} were attributed to the different types of C−H bonds.[52]

The length (height) of the grown nanotubes was measured using the Ambios XP- 1 Stylus Profiler. By scanning the transition edge of grown nanotubes on the substrate, the length of the CNTs was recorded to be about 49 nm, corresponding to 3 h of the duration of the growth process (Figure S5). The growth rate corresponding to these values was 0.27 nm·min^{-1}, which was slow enough to obtain nanotubes with a length of micrometers. The length value of the nanotubes directly depends on the duration of the growth process when all the typical growth parameters are kept constant, or the growth rate can also be increased by increasing the power of the generator over a certain range (up to 200 W).

The CNTs/Si sample was investigated by the elementary EDX analysis. The well-appearing peaks of the C, O, and Si elements are reflected in Figure S6, presented in their weight and atomic percentages. The actual concentrations of C and O materials in the CNTs/Si sample were 9.22 and 4.11 wt %, respectively. It is clear that the presence of a large amount of silicon (86.67 wt %) was due to the silicon substrate because, in the case of the very small thickness (height) of nanotubes, the electron beam penetrated the substrate during the EDX measurement. The presence of oxygen was believed to be due to the prior adsorption of certain oxygen species from the environment onto the silicon surface.

https://doi.org/10.1021/acsomega.3c01705
ACS Omega 2023, 8, 20949−20958

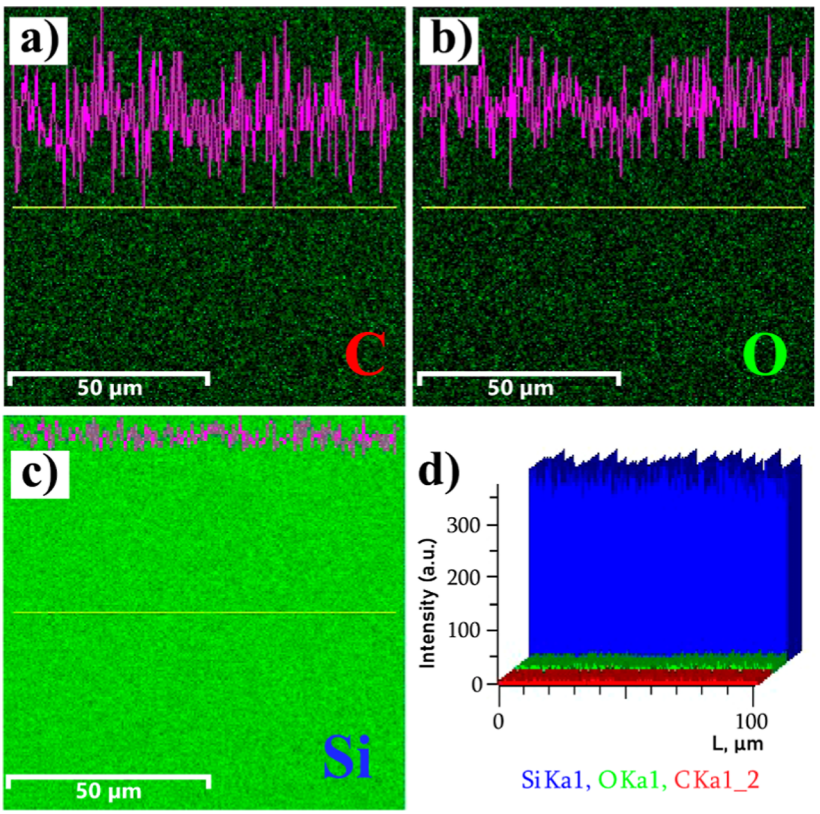

Figure 5. EDX elemental mapping analysis of C (a), O (b), and Si (c) elements and X-ray intensity of characteristic lines (d).

Elemental mapping analysis was also carried out for the CNTs/Si sample by EDX spectroscopy. The e-mapped images with a clearly uniform distribution of C, O, and Si elements differing in their colors and distinctive characteristic lines of X-ray intensity are presented in Figure 5.

For the sensitization of the grown CNTs toward PGV, the Fe_2O_3:ZnO composite material was deposited onto the CNTs/Si(100) surface; therefore, the characteristics of this material were also investigated by the transmission electron microscopy (TEM) technique. The hexagonal shape of the ZnO material and the interplanar spacing in the crystals are clearly visible (Figure 6).

Elemental mapping analysis was also performed for the Fe_2O_3:ZnO composite material, confirming the nearly uniform distribution of Fe, Zn, and O elements (Figure S7).

Gas-Sensing Studies. The gas-sensing characteristics of the Fe_2O_3:ZnO/CNTs sensor were carefully investigated toward PGV, considering also the possible influence of UV irradiation on them. First, the effect of operating temperature on the sensor response was studied combined with UV light. From RT to 100 °C, the sensor did not show sensitivity to PGV with and without UV rays, while at 150 °C the sensor response was quite noticeable (Figure 7a). The sensor showed a maximum response to 60 ppm PGV at 300 and 250 °C with and without UV light, respectively. Although the maximum response value (60) obtained under the influence of UV at 300 °C was more than 1.6 times higher than that at 250 °C without UV light (37), we chose the 200−250 °C interval as the optimal operating temperature range without UV assistance. In this temperature range, UV rays hardly improved the sensor characteristics and their application to the active surface of the sensor was not justified. Furthermore, the sensor operation at 300 °C combined with UV irradiation requires a higher power consumption, which is not very beneficial for this type of sensor. Sensor performance indicators attributed to recovery and response times were also evaluated with and without UV light. UV exposure did not significantly improve the sensor's performance; instead, the increase in temperature resulted in a significant reduction in response and recovery times (Figure 7b,c).

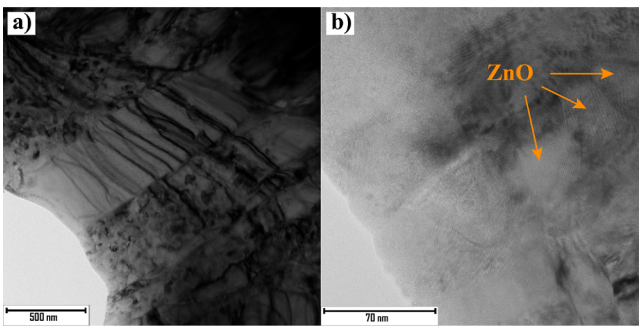

Figure 6. Low- (a) and high- (b) resolution TEM images for the Fe_2O_3:ZnO material.

By heating the sensor from 150 to 350 °C, the recovery time essentially improved in both with and without UV irradiation conditions. Recovery time decreased from 40.3 min to 47 s and from 44.1 min to 23 s with and without UV irradiation, respectively, by sweeping the sensor temperature from 150 to 350 °C. Response time was also improved in both UV-on and UV-off regimes after the sensor heating in this interval. From the obtained measurements, the range of response and recovery times of the sensor without UV irradiation can be attributed to 13−114 and 140−2600 s at 250 and 200 °C,

https://doi.org/10.1021/acsomega.3c01705
ACS Omega 2023, 8, 20949−20958

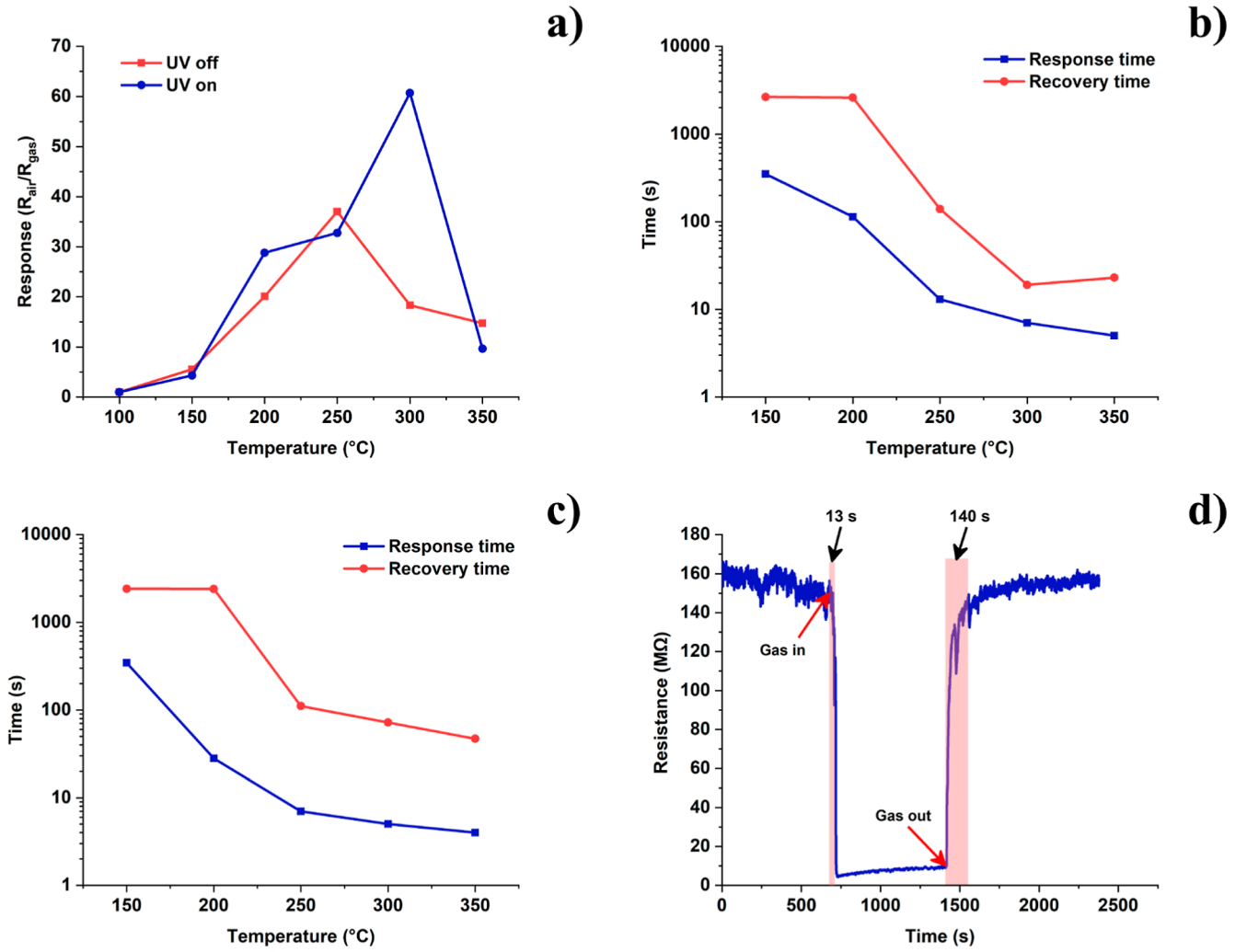

Figure 7. (a) Sensor response vs operating temperature with and without UV irradiation at 60 ppm PGV, dependences of response and recovery times on operating temperature with (b) and without (c) UV irradiation at 60 ppm PGV, and (d) real-time resistance curve of the sensor at 60 ppm PGV representing the response and recovery times.

respectively, which were quite satisfactory values. Choosing as optimal operating temperatures, all additional measurements were recorded at 200 and 250 °C without UV rays. The real-time resistance curve of the sensor toward 60 ppm PGV representing the response and recovery time without UV irradiation at 250 °C is presented in Figure 7d providing an accurate estimate of the sensor's speed. The response and recovery times of the sensor were 13 and 140 s, respectively, presenting a fairly fast performance characteristic. The long response time is assumed to be due to the slowing down of the desorption of the gas molecules from the intergranular area and CNTs.

In order to reveal the low detection limit of the sensor and the entire range of detecting concentrations, the characteristics of the baseline resistance change of the sensor at different concentrations of PGV were investigated. The real-time response curves of the sensors were extracted toward PGV in the range of 1.5−140 ppm, exhibiting fairly clear recovery/response characteristics at both 200 and 250 °C (Figure 8a,b). The sensor response increased linearly from a value of 2.5−30 at 200 °C when the PGV concentration was increased from 1.5 to 140 ppm, showing an extremely low gas detection limit (1.5 ppm). Almost the same behavior was manifested at 250 °C, while at this temperature, the response values were found in higher ranges (5−105). At higher PGV concentrations, the stabilization of the sensor in a gas environment was somewhat difficult since the adsorption of a large number of gas molecules on the sensing surface tends to take a longer response time.

The linearity of the sensor results in a linear dependence of the sensor response on the gas concentration, which allows the sensor to be used in detectors as a sophisticated gas alarming system. In the case of seven different concentrations of PGV (in a range of 1.5−140 ppm), the sensor response was recorded and its dependence on the gas concentration was removed, presenting nearly linear characteristics at both 200 and 250 °C (Figure 8c). This will allow the Fe_2O_3:ZnO/CNTs sensor to be more easily used as a device for measuring PGV concentrations and making approximations over a wider range of concentrations.

The repeatability of the sensor response is critical for long-term sensor performance and reliable signal generation in safety control systems. The repeatability tests of the sensor for PGV at 200 and 250 °C are presented in Figure S8a,b, respectively. At both temperatures, the sensor showed almost the same characteristic of the dynamic resistance curves

https://doi.org/10.1021/acsomega.3c01705
ACS Omega 2023, 8, 20949−20958

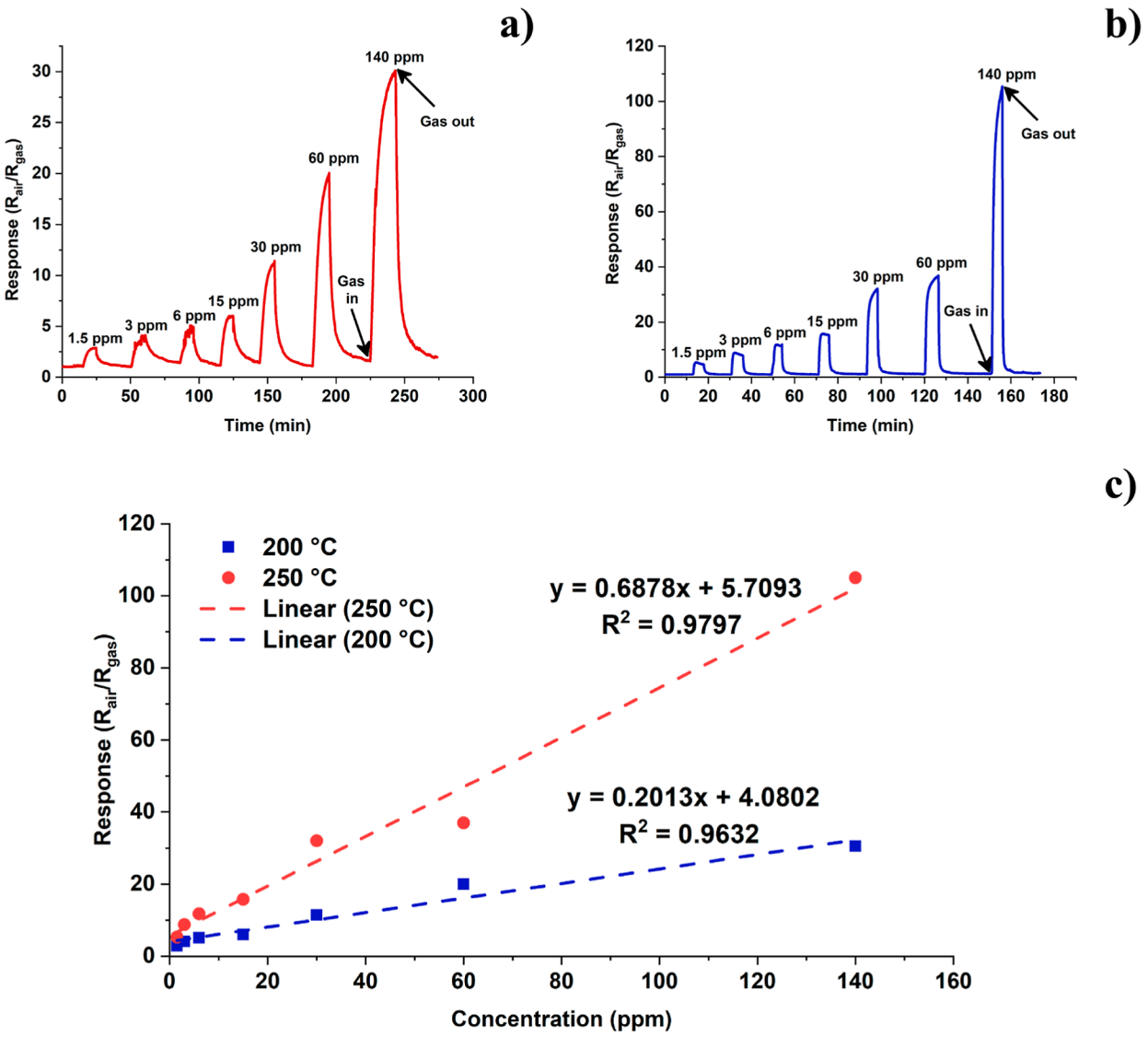

Figure 8. Dynamic resistance curves of the sensor to different concentrations of PGV at 200 °C (a) and 250 °C (b) and PGV response vs concentration at 200 and 250 °C (c).

measured in six different experiments, providing high repeatability of the sensor response. The slight deviation of the sensor baseline resistance to a lower range of resistances is assumed to be related to the incomplete desorption of preabsorbed gas molecules after exposure to the gas. This process is also facilitated by the slow desorption rate of gas molecules diffused within the pores and CNTs of the sensitive film. The cross-sensitivity of the sensor to other types of gases, such as toluene, ammonia, water, ethanol, hydrogen peroxide vapor (HPV), acetone, and dimethylformamide (DMF), was also tested. The sensor response to 60 ppm PGV was compared to that of 320 ppm toluene, 130 ppm ammonia, 3300 ppm water, 675 ppm ethanol, 225 ppm HPV, 400 ppm acetone, and 340 ppm DMF at both 200 and 250 °C (Figure S8c,d). The response values of the nontarget gases were in the ranges of 1.4−4 and 1−4.4 at 200 and 250 °C, respectively, which are definitely incomparably lower than those of PGV for a much lower concentration (60 ppm). This is truly a testament to the high selectivity of the sensor, making it suitable for use in real and natural environments.

The temporal stability of the sensor was consistently tested for 3 months from the initial measurements. The experiment showed that during this testing period, not only the response but also the baseline resistance and the response/recovery times of the sensor did not have any significant changes from their initial values. The response to 60 ppm of PGV decreased from its preliminary value by 0.8% reaching a value of 36.7 from 37. The sensor baseline resistance was decreased by 1.4%, and response and recovery times were increased by approximately 2 and 1.5%, respectively, at 250 °C operating temperature.

Sensors based on pristine CNTs and Fe_2O_3:ZnO have also been fabricated. The sensitivities of the CNTs/Si(100) and Fe_2O_3:ZnO sensors to PGV were extremely low, which proves the need for a composite combination of these two materials as an advanced sensor structure, especially useful for PGV detection.

In earlier published work,[36] the MWCNTs/SnO_2 PGV sensor showed a significantly higher low detection limit (13 ppm) and a lower sensitivity (S = 1.5 for 13 ppm), while our

https://doi.org/10.1021/acsomega.3c01705
ACS Omega 2023, 8, 20949−20958

Fe_2O_3:ZnO/CNTs sensor exhibited a response of 15.8 toward 15 ppm PGV.

The sensing mechanism of chemoresistive gas sensors is mainly the result of chemical reactions between the gas molecules and the semiconductor lattice on the sensitive surface. Typically, oxygen species are adsorbed from the atmosphere onto the semiconductor surface and chemisorbed under sufficient temperature conditions. This is accompanied by the transformation of neutral oxygen species into ions, which are localized on the active surface. As a result, a sufficient number of electrons are taken from the lattice and an electron depletion layer of near-surface area is formed. When the target gas molecules ($C_3H_8O_2$) reach the active surface, they dissociate mainly due to the availability of thermal energy around the spillover zones and the resulting species react with the localized oxygen ions. As a result, oxygen ions are withdrawn from the surface, and previously absorbed electrons return to the semiconductor. This leads to a decrease in the resistance of the sensor under the influence of the target gas, which is the signal of the sensor itself.[53−55]

The effective combination of CNTs and Fe_2O_3:ZnO material resulted in the high sensitivity of the Fe_2O_3:ZnO/CNTs sensor to PGV, as the nanotubes mainly increase the effective surface area of the sensing material and the metal oxide nanoparticles are generally responsible for the gas/solid film interaction effects.[56,57]

CONCLUSIONS

In summary, we have used the RF magnetron sputtering method to synthesize vertically aligned CNT arrays. Unlike the ragged sides of the Si substrates, vertically aligned CNTs were successfully grown on the smoothed surface of the Si(100) substrate confirmed by the SEM images. The diameters of the homogeneously distributed CNTs were in the range of 15−25 nm, with 49 nm in height (length). The presence of D (1367 cm^{-1}) and G (1580 cm^{-1}) bands as a typical characteristic of the formation of CNTs was confirmed by Raman spectroscopy almost coinciding with well-pronounced intensity peaks of 1192 and 1608 cm^{-1} in the FTIR spectrum, respectively. We also manufactured and investigated a PGV sensor based on the Fe_2O_3:ZnO/CNTs material with the Pt interdigitated electrodes. The presence of UV rays did not significantly affect the gas-sensing behavior, even in combination with thermal heating. The sensor response increased linearly from 5 to 105 at 250 °C when increasing the PGV concentration from 1.5 to 140 ppm, demonstrating an extremely low PGV detection limit (1.5 ppm). The Fe_2O_3:ZnO/CNTs sensor with a response time of 13 s and a recovery time of 140 s demonstrated high selectivity and response repeatability, strongly justifying the use of this structure as a PGV sensor.

ASSOCIATED CONTENT

Supporting Information

The Supporting Information is available free of charge at https://pubs.acs.org/doi/10.1021/acsomega.3c01705.

Actual photographs of the High-Vacuum Magnetron Plasma System and gas sensor testing system, Raman spectra of the CNTs/Si, FTIR spectrum of the CNTs/Si sample, measured length of the CNTs, EDX spectrum of the CNTs/Si sample, TEM image and elemental mapping analysis of the Fe_2O_3/ZnO material, and results of repeatability and selectivity of the sensor (PDF)

AUTHOR INFORMATION

Corresponding Author

Artak Sayunts − *Center of Semiconductor Devices and Nanotechnologies, Yerevan State University, 0025 Yerevan, Armenia;* orcid.org/0000-0003-3898-9996; Email: sayuntsartak@ysu.am

Authors

Mikayel Aleksanyan − *Center of Semiconductor Devices and Nanotechnologies, Yerevan State University, 0025 Yerevan, Armenia*

Gevorg Shahkhatuni − *Center of Semiconductor Devices and Nanotechnologies, Yerevan State University, 0025 Yerevan, Armenia*

Zarine Simonyan − *Center of Semiconductor Devices and Nanotechnologies, Yerevan State University, 0025 Yerevan, Armenia*

Hayk Kasparyan − *Department of Mathematics, Informatics and Cybernetics, Faculty of Chemical Engineering, University of Chemistry and Technology Prague, 166 28 Prague, Czech Republic*

Dušan Kopecký − *Department of Mathematics, Informatics and Cybernetics, Faculty of Chemical Engineering, University of Chemistry and Technology Prague, 166 28 Prague, Czech Republic*

Complete contact information is available at: https://pubs.acs.org/10.1021/acsomega.3c01705

Author Contributions

The manuscript was written through contributions of all authors. All authors have given approval to the final version of the manuscript.

Notes

The authors declare no competing financial interest.

ACKNOWLEDGMENTS

This research was funded by the Science Committee of RA, grant no. 21SCG-2J001. G. Badalyan helped for measurements of elemental mapping and the thickness of the sample.

REFERENCES

(1) Xu, X.; Huang, S.; Hu, Y.; Lu, J.; Yang, Z. Continuous synthesis of carbon nanotubes using a metal-free catalyst by CVD. *Mater. Chem. Phys.* **2012**, *133*, 95−102.

(2) Xiao, Z.; Wang, X.; Meng, J.; Wang, H.; Zhao, Y.; Mai, L. Advances and perspectives on one-dimensional nanostructure electrode materials for potassium-ion batteries. *Mater. Today* **2022**, *56*, 114−134.

(3) Soni, S. K.; Thomas, B.; Kar, V. R. A Comprehensive Review on CNTs and CNT-Reinforced Composites: Syntheses, Characteristics and Applications. *Mater. Today Commun.* **2020**, *25*, 101546.

(4) Kholghi Eshkalak, S.; Chinnappan, A.; Jayathilaka, W. A. D. M.; Khatibzadeh, M.; Kowsari, E.; Ramakrishna, S. A review on inkjet printing of CNT composites for smart applications. *Appl. Mater. Today* **2017**, *9*, 372−386.

(5) Gupta, S.; Pramanik, S.; Smita; Das, S. K.; Saha, S. Dynamic analysis of wave propagation and buckling phenomena in carbon nanotubes (CNTs). *Wave Motion* **2021**, *104*, 102730.

(6) Kuramochi, H.; Manago, T.; Koltsov, D.; Takenaka, M.; Iitake, M.; Akinaga, H. Advantages of CNT−MFM probes in observation of

domain walls of soft magnetic materials. *Surf. Sci.* **2007**, *601*, 5289−5293.
(7) Niu, M.; Zhao, Y.; Sui, C.; Sang, Y.; Hao, W.; Li, J.; He, X.; Wang, C. Mechanical properties of twisted CNT fibers: A molecular dynamic study. *Mater. Today Commun.* **2023**, *34*, 105378.
(8) Meng, A.; Hong, X.; Zhang, Y.; Liu, W.; Zhang, Z.; Sheng, L.; Li, Z. A free-standing flexible sensor MnO_2−Co/rGO-CNT for effective electrochemical hydrogen peroxide sensing and real-time cancer biomarker assaying. *Ceram. Int.* **2023**, *49*, 2440−2450.
(9) Loghin, F. C.; Falco, A.; Moreno-Cruz, F.; Lugli, P.; Morales, D. P.; Salmerón, J. F.; Rivadeneyra, A. Facile manufacturing of sub-mm thick CNT-based RC filters. *Mater. Lett.* **2021**, *297*, 129939.
(10) Son, W.; Lee, D. W.; Kim, Y. K.; Chun, S.; Lee, J. M.; Choi, J. H.; Shim, W. S.; Suh, D.; Lim, S. K.; Choi, C. PdO-Nanoparticle-Embedded Carbon Nanotube Yarns for Wearable Hydrogen Gas Sensing Platforms with Fast and Sensitive Responses. *ACS Sens.* **2023**, *8*, 94−102.
(11) Ingtipi, K.; Choudhury, B. J.; Moholkar, V. S. Ultrasound assisted lignin-decorated MWCNT doped flexible PVA−Chitosan composite hydrogel. *Mater. Today Commun.* **2023**, *35*, 105676.
(12) Liu, X.; Fan, L.; Wang, Y.; Zhang, W.; Ai, H.; Wang, Z.; Zhang, D.; Jia, H.; Wang, C. Nanofiber-based $Sm_{0.5}Sr_{0.5}Co_{0.2}Fe_{0.8}O_{3-\delta}$/N-MWCNT composites as an efficient bifunctional electrocatalyst towards OER/ORR. *Int. J. Hydrogen Energy* **2023**, *48*, 15555−15565 Article ASAP.
(13) Jia, Y.; Zhang, Y.; Zhang, X.; Cheng, J.; Xie, Y.; Zhang, Y.; Yin, X.; Song, F.; Cui, H. Novel CdS/PANI/MWCNTs photocatalysts for photocatalytic degradation of xanthate in wastewater. *Sep. Purif. Technol.* **2023**, *309*, 123022.
(14) Momin, Z. H.; Ahmad, A. T. A.; Malkhede, D. D.; Koduru, J. R. Synthesis of thin-film composite of MWCNTs-polythiophene-Ru/Pd at liquid-liquid interface for supercapacitor application. *Inorg. Chem. Commun.* **2023**, *149*, 110434.
(15) Gayathri, V.; Praveen, E.; Jayakumar, K.; Karazhanov, S.; Mohan, R. C. Graphene quantum dots assisted $CuCo_2S_4$/MWCNT nanoflakes as superior bifunctional electrocatalysts for dye-sensitized solar cell and supercapacitor applications. *Colloids surf., A* **2023**, *662*, 130948.
(16) Zhang, K.; Qin, R.; Chen, S.; Liu, X.; Liu, Y. Customizing defect location in MWCNTs/Fe_3O_4 composites by direct fluorination for enhancing microwave absorption performance. *Appl. Surf. Sci.* **2023**, *612*, 155860.
(17) Yadav, M. D.; Patwardhan, A. W.; Joshi, J. B.; Dasgupta, K. Selective synthesis of metallic and semi-conducting single-walled carbon nanotube by floating catalyst chemical vapour deposition. *Diamond Relat. Mater.* **2019**, *97*, 107432.
(18) Chen, S.-Z.; Xie, F.; Ning, F.; Liu, Y.-Y.; Zhou, W.-X.; Yu, J.-F.; Chen, K.-Q. Breaking surface states causes transformation from metallic to semi-conducting behavior in carbon foam nanowires. *Carbon* **2017**, *111*, 867−877.
(19) Wang, Y.; Liu, Y.; Yang, H.; Liu, Y.; Wu, K.-H.; Yang, G. Ionic liquid derived Fe, N, B co-doped bamboo-like carbon nanotubes as an efficient oxygen reduction catalyst. *J. Colloid Interface Sci.* **2020**, *579*, 637−644.
(20) Giannakopoulou, T.; Pilatos, G.; Todorova, N.; Boukos, N.; Vaimakis, T.; Karatasios, I.; Trapalis, C. Effect of processing temperature on growing bamboo-like carbon nanotubes by chemical vapor deposition. *Mater. Today Chem.* **2021**, *19*, 100388.
(21) Borowiak-Palen, E.; Rümmeli, M. H. Activated Cu catalysts for alcohol CVD synthesized non-magnetic bamboo-like carbon nanotubes and branched bamboo-like carbon nanotubes. *Superlattices Microstruct.* **2009**, *46*, 374−378.
(22) Brown, B.; Parker, C. B.; Stoner, B. R.; Glass, J. T. Growth of vertically aligned bamboo-like carbon nanotubes from ammonia/methane precursors using a platinum catalyst. *Carbon* **2011**, *49*, 266−274.
(23) Lee, K.-Y.; Ikuno, T.; Tsuji, K.; Ohkura, S.; Honda, S.; Katayama, M.; Oura, K.; Hirao, T. Synthesis of aligned bamboo-like carbon nanotubes using radio frequency magnetron sputtering. *J. Vac. Sci. Technol., B: Microelectron. Nanometer Struct.–Process., Meas., Phenom.* **2003**, *21*, 1437.
(24) Homayoonnia, S.; Phani, A.; Kim, S. MOF/MWCNT−Nanocomposite Manipulates High Selectivity to Gas via Different Adsorption Sites with Varying Electron Affinity: A Study in Methane Detection in Parts-per-Billion. *ACS Sens.* **2022**, *7*, 3846−3856.
(25) Alheshibri, M.; Elsayed, K.; Haladu, S. A.; Magami, S. M.; Al Baroot, A.; Ercan, I.; Ercan, F.; Manda, A. A.; Çevik, E.; Kayed, T. S.; Alsanea, A. A.; Alotaibi, A. M.; Al-Otaibi, A. L. Synthesis of Ag nanoparticles-decorated on CNTs/TiO_2 nanocomposite as efficient photocatalysts via nanosecond pulsed laser ablation. *Opt. Laser Technol.* **2022**, *155*, 108443.
(26) Soni, G.; Jain, K.; Soni, P.; Jangir, R. K.; Vijay, Y. K. Synthesis of multiwall carbon nanotubes in presence of magnetic field using underwater arc discharge system. *Mater. Today Proc.* **2020**, *30*, 225−228.
(27) Poli, A.; Dagher, G.; Santos, A. F.; Baldoni-Andrey, P.; Jacob, M.; Batiot-Dupeyrat, C.; Teychené, B. Impact of C-CVD synthesis conditions on the hydraulic and electronic properties of SiC/CNTs nanocomposite microfiltration membranes. *Diamond Relat. Mater.* **2021**, *120*, 108611.
(28) Lin, J.; Yang, Y.; Zhang, H.; LI, F.; Huang, G.; Wu, C. Preparation of CNT−Co@TiB_2 by catalytic CVD: Effects of synthesis temperature and growth time. *Diamond Relat. Mater.* **2020**, *106*, 107830.
(29) Lin, J.; Yang, Y.; Zhang, H.; LI, F. Effect of source gases on CVD synthesis of CNTs@TiB_2 composite powders using Ni/Y_2O_3 as the catalyst. *Ceram. Int.* **2020**, *46*, 10704−10709.
(30) Cai, X.; Cong, H.; Liu, C. Synthesis of vertically-aligned carbon nanotubes without a catalyst by hydrogen arc discharge. *Carbon* **2012**, *50*, 2726−2730.
(31) Pasha, M. A.; Poursalehi, R.; Vesaghi, M. A.; Shafiekhani, A. The effect of temperature on the TCVD growth of CNTs from LPG over Pd nanoparticles prepared by laser ablation. *Phys. B* **2010**, *405*, 3468−3474.
(32) Scalese, S.; Scuderi, V.; Simone, F.; Pennisi, A.; Privitera, V. Ex situ and in situ catalyst deposition for CNT synthesis by RF-magnetron sputtering. *Phys. E* **2008**, *40*, 2243−2246.
(33) Scalese, S.; Scuderi, V.; Simone, F.; Pennisi, A.; Compagnini, G.; Bongiorno, C.; Privitera, V. Carbon aligned nanocolumns by RF-Magnetron sputtering: The influence of the growth parameters. *Phys. E* **2007**, *37*, 231−235.
(34) Agoons, D. D.; Agoons, B. B.; Emmanuel, K. E.; Matawalle, F. A.; Cunningham, J. M. Association between electronic cigarette use and fragility fractures among US adults. *Am. J. Med. Open* **2021**, *1*−*6*, 100002.
(35) Jackson, G.; Roberts, R. T.; Wainwright, T. Mechanism of Beer Foam Stabilization by Propylene Glycol Alginate. *J. Inst. Brew.* **1980**, *86*, 34−37.
(36) Adamyan, Z.; Sayunts, A.; Aroutiounian, V.; Khachaturyan, E.; Vrnata, M.; Fitl, P.; Vlček, J. Nanocomposite sensors of propylene glycol, dimethylformamide and formaldehyde vapors. *J. Sens. Sens. Syst.* **2018**, *7*, 31−41.
(37) Okolie, J. A. Insights on production mechanism and industrial applications of renewable propylene glycol. *iScience* **2022**, *25*, 104903.
(38) Jiménez, R. X.; Young, A. F.; Fernandes, H. L. S. Propylene glycol from glycerol: Process evaluation and break-even price determination. *Renewable Energy* **2020**, *158*, 181−191.
(39) Aleksanyan, M. S.; Sayunts, A. G.; Shahkhatuni, G. H.; Simonyan, Z. G.; Aroutiounian, V. M.; Shahnazaryan, G. E. Flexible sensor based on multi-walled carbon nanotube-SnO_2 nanocomposite material for hydrogen detection. *Adv. Nat. Sci.: Nanosci. Nanotechnol.* **2022**, *13*, 035003.
(40) Aleksanyan, M. S.; Sayunts, A. G.; Shahkhatuni, G. H.; Simonyan, Z. G.; Aroutiounian, V. M.; Shahnazaryan, G. E. Flexible SnO_2⟨Co⟩/MWCNT Sensor for Detection Low Concentrations of Hydrogen Peroxide Vapors. *J. Contemp. Phys.* **2022**, *57*, 133−139.
(41) Aroutiounian, V. M.; Arakelyan, V. M.; Khachaturyan, E. A.; Shahnazaryan, G. E.; Aleksanyan, M. S.; Forro, L.; Magrez, A.;

https://doi.org/10.1021/acsomega.3c01705
ACS Omega 2023, 8, 20949−20958

Hernadi, K.; Nemeth, Z. Manufacturing and investigations of i-butane sensor made of SnO_2/multiwall-carbon-nanotube nanocomposite. *Sens. Actuators, B* **2012**, *173*, 890−896.
(42) Leghrib, R.; Felten, A.; Pireaux, J. J.; Llobet, E. Gas sensors based on doped-CNT/SnO_2 composites for NO_2 detection at room temperature. *Thin Solid Films* **2011**, *520*, 966−970.
(43) Feng, B.; Feng, Y.; Li, Y.; Su, Y.; Deng, Y.; Wei, J. Synthesis of Mesoporous Ag_2O/SnO_2 Nanospheres for Selective Sensing of Formaldehyde at a Low Working Temperature. *ACS Sens.* **2022**, *7*, 3963−3972.
(44) Lim, Y. D.; Avramchuck, A. V.; Grapov, D.; Tan, C. W.; Tay, B. K.; Aditya, S.; Labunov, V. Enhanced Carbon Nanotubes Growth Using Nickel/Ferrocene-Hybridized Catalyst. *ACS Omega* **2017**, *2*, 6063−6071.
(45) Allaedini, G.; Tasirin, S. M.; Aminayi, P.; Yaakob, Z.; MeowTalib, M. Z. Carbon Nanotubes via Different Catalysts and the Important Factors That Affect Their Production: A Review on Catalyst Preferences. *Int. J. Nano Dimens.* **2016**, *7*, 186−200.
(46) Moisala, A.; Nasibulin, A. G.; Kauppinen, E. I. The role of metal nanoparticles in the catalytic production of single-walled carbon nanotubes—a review. *J. Phys.: Condens. Matter* **2003**, *15*, S3011−S3035.
(47) Aleksanyan, M.; Sayunts, A.; Shahkhatuni, G.; Simonyan, Z.; Kasparyan, H.; Kopecký, D. Room Temperature Detection of Hydrogen Peroxide Vapor by Fe_2O_3:ZnO Nanograins. *Nanomaterials* **2022**, *13*, 120.
(48) Aleksanyan, M.; Sayunts, A.; Shahkhatuni, G.; Simonyan, Z.; Shahnazaryan, G.; Aroutiounian, V. Gas Sensor Based on ZnO Nanostructured Film for the Detection of Ethanol Vapor. *Chemosensors* **2022**, *10*, 245.
(49) Melvin, G. J. H.; Ni, Q.-Q.; Suzuki, Y.; Natsuki, T. Microwave-absorbing properties of silver nanoparticle/carbon nanotube hybrid nanocomposites. *J. Mater. Sci.* **2014**, *49*, 5199−5207.
(50) Kim, K. H.; Lee, D. J.; Cho, K. M.; Kim, S. J.; Park, J.-K.; Jung, H.-T. Complete magnesiothermic reduction reaction of vertically aligned mesoporous silica channels to form pure silicon nanoparticles. *Sci. Rep.* **2015**, *5*, 9014.
(51) Lehman, J. H.; Terrones, M.; Mansfield, E.; Hurst, K. E.; Meunier, V. Evaluating the characteristics of multiwall carbon nanotubes. *Carbon* **2011**, *49*, 2581−2602.
(52) Fayazfar, H.; Afshar, A.; Dolati, A. Controlled Growth of Well-Aligned Carbon Nanotubes, Electrochemical Modification and Electrodeposition of Multiple Shapes of Gold Nanostructures. *Mater. Sci. Appl.* **2013**, *04*, 667−678.
(53) Acharyya, S.; Nag, S.; Kimbahune, S.; Ghose, A.; Pal, A.; Guha, P. K. Selective Discrimination of VOCs Applying Gas Sensing Kinetic Analysis over a Metal Oxide-Based Chemiresistive Gas Sensor. *ACS Sens.* **2021**, *6*, 2218−2224.
(54) Jian, Y.; Hu, W.; Zhao, Z.; Cheng, P.; Haick, H.; Yao, M.; Wu, W. Gas Sensors Based on Chemi-Resistive Hybrid Functional Nanomaterials. *Nano-Micro Lett.* **2020**, *12*, 71.
(55) Wetchakun, K.; Samerjai, T.; Tamaekong, N.; Liewhiran, C.; Siriwong, C.; Kruefu, V.; Wisitsoraat, A.; Tuantranont, A.; Phanichphant, S. Semiconducting metal oxides as sensors for environmentally hazardous gases. *Sens. Actuators, B* **2011**, *160*, 580−591.
(56) Septiani, N. L. W.; Yuliarto, B. Review—The Development of Gas Sensor Based on Carbon Nanotubes. *J. Electrochem. Soc.* **2016**, *163*, B97−B106.
(57) Tasaltin, C.; Basarir, F. Preparation of flexible VOC sensor based on carbon nanotubes and gold nanoparticles. *Sens. Actuators, B* **2014**, *194*, 173−179.

https://doi.org/10.1021/acsomega.3c01705
ACS Omega 2023, 8, 20949−20958